ENVIRONMENTAL RESEARCH
LETTERS

LETTER • **OPEN ACCESS**

Evaluating the potential of iron-based interventions in methane reduction and climate mitigation

To cite this article: Daphne Meidan *et al* 2024 *Environ. Res. Lett.* **19** 054023

ENVIRONMENTAL RESEARCH
LETTERS

LETTER

Evaluating the potential of iron-based interventions in methane reduction and climate mitigation

Daphne Meidan[1], **Qinyi Li**[2], **Carlos A Cuevas**[3], **Scott C Doney**[4], **Rafael P Fernandez**[5], **Maarten M J W van Herpen**[6], **Matthew S Johnson**[7], **Douglas E Kinnison**[8], **Longlei Li**[1], **Douglas S Hamilton**[9], **Alfonso Saiz-Lopez**[3], **Peter Hess**[10] **and Natalie M Mahowald**[1,*]

[1] Department of Earth and Atmospheric Sciences, Atkinson Center for a Sustainable Future, Cornell University, Ithaca, NY, United States of America
[2] Environment Research Institute, Shandong University, Qingdao, People's Republic of China
[3] Department of Atmospheric Chemistry and Climate, Institute of Physical Chemistry Blas Cabrera, CSIC, Madrid 28006, Spain
[4] Department of Environmental Sciences, University of Virginia, Charlottesville, VA, United States of America
[5] Institute for Interdisciplinary Science (ICB), National Research Council (CONICET), FCEN-UNCuyo, Mendoza, Argentina
[6] Acacia Impact Innovation BV, Acacialaan 9, 5384 BB Heesch, The Netherlands
[7] Department of Chemistry, University of Copenhagen, Universitetsparken 5, DK-2100 Copenhagen Ø, Denmark
[8] Climate and Global Dynamics Laboratory, National Center for Atmospheric Research, Boulder, CO, United States of America
[9] Marine, Earth, and Atmospheric Sciences, North Carolina State University, Raleigh, NC, United States of America
[10] Department of Biological and Environmental Engineering, Cornell University, Ithaca, NY, United States of America
* Author to whom any correspondence should be addressed.

E-mail: mahowald@cornell.edu

Keywords: methane oxidation, chlorine chemistry, community earth system model (CESM), iron aerosols

Supplementary material for this article is available online

OPEN ACCESS

RECEIVED
30 October 2023

REVISED
4 April 2024

ACCEPTED FOR PUBLICATION
11 April 2024

PUBLISHED
19 April 2024

Abstract

Keeping global surface temperatures below international climate targets will require substantial measures to control atmospheric CO_2 and CH_4 concentrations. Recent studies have focused on interventions to decrease CH_4 through enhanced atmospheric oxidation. Here for the first time using a set of models, we evaluate the effect of adding iron aerosols to the atmosphere to enhance molecular chlorine production, and thus enhance the atmospheric oxidation of methane and reduce its concentration. Using different iron emission sensitivity scenarios, we examine the potential role and impact of enhanced iron emissions on direct interactions with solar radiation, and on the chemical and radiative response of methane. Our results show that the impact of iron emissions on CH_4 depends sensitively on the location of the iron emissions. In all emission regions there is a threshold in the amount of iron that must be added to remove methane. Below this threshold CH_4 increases. Even once that threshold is reached, the iron-aerosol driven chlorine-enhanced impacts on climate are complex. The radiative forcing of both methane and ozone are decreased in the most efficient regions but the direct effect due to the addition of absorbing iron aerosols tends to warm the planet. Adding any anthropogenic aerosol may also cool the planet due to aerosol cloud interactions, although these are very uncertain, and here we focus on the unique properties of adding iron aerosols. If the added emissions have a similar distribution as current shipping emissions, our study shows that the amount of iron aerosols that must be added before methane decreases is 2.5 times the current shipping emissions of iron aerosols, or 6 Tg Fe yr^{-1} in the most ideal case examined here. Our study suggests that the photoactive fraction of iron aerosols is a key variable controlling the impact of iron additions and poorly understood. More studies of the sensitivity of when, where and how iron aerosols are added should be

conducted. Before seriously considering this method, additional impacts on the atmospheric chemistry, climate, environmental impacts and air pollution should be carefully assessed in future studies since they are likely to be important.

1. Introduction

Controlling atmospheric concentrations of methane (CH_4) is a critical and complex challenge to address climate change (IPCC Core writing team 2023). Methane is a potent greenhouse gas that contributes significantly to global warming due to its high radiative forcing (RF) and heat-trapping capabilities (Intergovernmental Panel on Climate Change (IPCC) 2023). Both natural and human activities contribute to methane emissions, and its atmospheric growth rate has been increasing since 2007 (IPCC 2021). Chemical reactions of methane with hydroxyl radicals (OH) and, to a lesser extent, atomic chlorine (Cl), are its main sinks in the atmospheric (Saunois *et al* 2020). It is largely the abundance of OH that determines the rate of methane oxidation and ultimately its chemical lifetime in the atmosphere. In addition to its role in global warming, methane also contributes to the formation of ozone, which also has direct implications for global warming, air pollution and human health, highlighting the idea that addressing methane can meet both air quality and climate goals (O'Grady 2021, United Nations Environment Programme and Climate and Clean Air Coalition 2021, Staniaszek *et al* 2022).

Recent research by (van Herpen *et al* 2023) has argued that there is link between North African mineral dust and chemical methane removal through a photocatalytic cycle for chlorine atom production, and that the proposed mineral dust-sea spray aerosols (MDSA) mechanism can explain the measurements of isotopes of carbon monoxide (CO) over the North Atlantic. More specifically, iron aerosols in the atmosphere catalyze the production of chlorine gas from sea salt aerosols through a complex photochemical process involving the release of Fe (III) chlorides, sunlight activation, and subsequent reoxidation, ultimately contributing to atmospheric halogen release (Wittmer *et al* 2015, Wittmer and Zetzsch 2017). This opens up the possibility of decreasing atmospheric methane by increasing the atmospheric production of chlorine (Cl) by adding iron aerosols (Dietrich Oeste *et al* 2017). Laboratory studies show that when sea salt and iron aerosols interact, iron chloride species are formed and can generate chlorine molecules (Cl_2) through photochemical reactions (Wittmer *et al* 2015, Wittmer and Zetzsch 2017, Mikkelsen *et al* 2024). Chlorine is highly reactive in the atmosphere, and will react with both ozone and methane, as well as other chemical species (Saiz-Lopez and von Glasow 2012, Wang *et al* 2019, Li *et al* 2023). The emissions of molecular chlorine (Cl_2) above the global ocean surface over a certain threshold (~90 Tg Cl yr^{-1}) have been shown to remove methane (Li *et al* 2023). However, below this threshold adding chlorine results in an unwanted increase of methane, attributed to the reaction of chlorine with ozone and the resulting decreased production of OH, the main chemical sink for methane (Horowitz *et al* 2020, Li *et al* 2023). However, if sufficient chlorine is added, this approach offers a potential pathway to decrease atmospheric methane levels.

Adding iron-containing aerosols to the atmosphere has significant environmental implications. Although the net radiative effect of iron-containing aerosols remains uncertain, they absorb short-wave solar radiation (Matsui *et al* 2018), contributing to climate-warming aerosols in the atmosphere. Aerosol cloud interactions (ACI) from added anthropogenic aerosols are well studied, but still highly uncertain (e.g. Kikstra *et al* 2022), and may also result from the addition of iron aerosols. In this paper we emphasize the iron aerosol specific impacts such as impact the radiative balance of the atmosphere through modifying cloud properties, leading to cooling through enhanced cloud brightening or warming through cloud burn-off (not quantified in this work) (Fan *et al* 2016). Aerosols such as iron are also air quality hazards (Lim *et al* 2012). Deposition of iron into the open ocean can stimulate phytoplankton productivity, impacting on ocean biogeochemistry (Moore *et al* 2006, 2013, Mahowald *et al* 2018, Ito *et al* 2021, Hamilton *et al* 2022). Thus, implementation of interventions such as adding iron to the atmosphere requires careful consideration, as the implications and potential side and indirect effects need to be thoroughly investigated.

In the atmosphere, iron primarily originates from desert dust aerosols (95%) which is approximately 3.5% iron, with about 5% of iron aerosols deriving from industrial, maritime shipping and biomass burning combustion sources (Mahowald *et al* 2008, Hamilton *et al* 2023). The current-day iron global emission from industrial and combustion sources is estimated to be 1.5–7.4 Tg Fe yr^{-1} (Ito and Miyakawa 2023). Iron in aerosols can have very different chemical states, from highly insoluble iron oxides, to more soluble iron in clays, to highly soluble iron in nanoparticles or other forms such as ferric sulphates (Shi *et al* 2009, Hamilton *et al* 2022). Soluble iron is thought to be the most relevant for ocean biogeochemistry, as it is more bioaccessible (Jickells *et al* 2005). In some regions of the open ocean, new primary production is limited by the low supply of bioavailable iron from the

combination of atmospheric deposition, recycling, and ocean upwelling and mixing (Moore *et al* 2013, Tagliabue *et al* 2017). Thus, there is the potential that additional ocean bioavailable iron input from an iron aerosol-CH_4 intervention could enhance regional ocean productivity and potentially the uptake of carbon dioxide (Jickells *et al* 2005, Hamilton *et al* 2022) because of the importance of atmospheric iron deposition to ocean biogeochemistry there has been substantial work on modeling and observations of soluble and total iron (e.g. Mahowald *et al* 2008, Myriokefalitakis *et al* 2018, Ito *et al* 2019). Photochemically active iron is more rarely studied, but is a fraction of soluble iron (Zhu *et al* 1997, Chen and Siefert 2003).

This study, for the first time, uses a set of global models to explore the complex relationship between iron emissions, molecular chlorine production, and their impact on methane abundance, with special emphasis on the potential effectiveness of iron sea salt aerosols as a methane removal mitigation strategy. Using different iron emission sensitivity scenarios, we examine the potential role and impact of iron emissions on direct interactions with solar radiation, and on the chemical and radiative response of methane. First, we explore the spatial effectiveness of different scenarios for iron emissions on atmospheric methane levels. We analyze the regional variations in methane removal efficiency from iron aerosols, classifying different regions based on the corresponding methane response. Second, we examine the relationship between iron emissions and molecular chlorine production, investigating the factors and regimes that control this important step of the process. Finally, we assess the potential changes in future RF and surface temperature due to additional iron emissions, in order to determine whether the anticipated benefits of iron emissions are substantial. Additionally, we highlight in the supplementary information the main uncertainties that should be considered when interpreting our findings.

2. Methods

2.1. Community earth system model description

In order to consider iron-chlorine-methane interactions we need: (i) a model of soluble atmospheric iron, (ii) a parameterization for the chlorine production from atmospheric soluble iron, and (iii) a model of atmospheric chlorine chemistry. These capabilities are available within the Community Earth System Model version 2 (CESM2) (Tilmes *et al* 2016, Danabasoglu *et al* 2020), although these components are not yet coupled together. Here, we use an asynchronous modeling approach where we first use the Mechanism of Intermediate complexity for modeling iron (MIMI) (Scanza *et al* 2018, Hamilton *et al* 2019) in CESM2 to simulate the distribution of soluble iron. MIMI is an improved atmospheric iron cycle module embedded within the Modal Aerosol Model version 4 (MAM4) (Liu *et al* 2016) that simulates the emission and atmospheric (acidic and organic) processing of iron in aerosols from both mineral dust and combustion sources. In particular, it simulates the time-evolving fraction of atmospheric iron that is soluble. The model includes dust and combustion iron emissions, which are transported in the model, and removed by wet and dry deposition (Hamilton *et al* 2019). The iron is divided into four types (slow reacting iron in dust, medium reacting iron in dust, industrial combustion iron, and fire iron) and each type is split into soluble and insoluble. For the optical properties of combustion soluble and insoluble iron we use the same optics as insoluble iron from mineral dust. Additional information on the iron optical properties can be found in the SI. More details on the iron species and their processing in the model can be found in (Hamilton *et al* 2019). The model utilizes CMIP6 inventory (2010) (Eyring *et al* 2016) for aerosol (except dust and sea salt aerosols that are modeled prognostically) and precursor gas emissions and MERRA data for meteorology (Rienecker *et al* 2011). The model uses prescribed sea surface temperature (SST) and a standard land model coupled to the atmosphere. Simulations are conducted at a spatial resolution of $1.25^\circ \times 0.9^\circ \times 56$ (longitude by latitude by vertical layers). The MIMI model has been carefully compared against observations in previous studies to simulate iron and soluble iron (Myriokefalitakis *et al* 2018, Conway *et al* 2019, Hamilton *et al* 2019, Myriokefalitakis 2019, Rathod *et al* 2020, Liu *et al* 2022). We simulate 4 years (2007–2010) and discard the first year as spin up, using the last 3 years for this study. The iron is added from combustion only above the ocean (i.e. iron from shipping), for both the soluble and insoluble iron species. Note that adding combustion iron as we do here is different from geoengineering proposals to spray $FeCl_3$ (Meyer-Oeste 2010, Dietrich Oeste *et al* 2017, Sturtz *et al* 2022, Mikkelsen *et al* 2024), a material that when photolyzed will produce photoactive iron (Mikkelsen *et al* 2024) and will have different evolution and effects than evaluated here.

Second, we calculate the Cl_2 production using the soluble iron global distribution as determined in MIMI and assuming instant mixing between the iron and sea salt aerosols (wherever the sea salt aerosol concentration is above 10^{-9} kg kg^{-1}). Note that this assumption will lead to an underestimate of the mixing and coagulation time scale (Carslaw 2022) and therefore an overestimation of the production. Additionally, for the Cl_2 production calculation we assume that the global percentage of photoactive iron to soluble iron is 31.6%, as was measured in Barbados (Zhu *et al* 1997). Laboratory studies show that when sea salt and iron aerosols combine in the presence of

light, iron chloride species are formed and can generate chlorine molecules (Cl_2) (Wittmer *et al* 2015, Wittmer and Zetzsch 2017, Mikkelsen *et al* 2024). We argue that it is only the photoactive iron that is able to produce chlorine (van Herpen *et al* 2023). While the limited observations suggest that photoactive iron is a subset of soluble iron, we do not know from field or laboratory studies the sources or attributes of photoactive iron. Here we simply assume the measured percentage at Barbados (Zhu *et al* 1997) holds everywhere. This approach was used in (van Herpen *et al* 2023) to simulate the impact of iron aerosols from dust on atmospheric methane, although (van Herpen *et al* 2023) assumed that 1.8% of iron is soluble and photoactive, while in the current study the soluble fraction as simulated in MIMI produces an average of about 2% photoactive iron (figure S2—soluble iron). Since the current suggested approach for decreasing atmospheric methane from iron additions is to add more iron to the exhaust from shipping (Dietrich Oeste *et al* 2017), we assume that the added iron has similar properties to the shipping iron currently included in the model. This allows the added iron to start out more soluble than dust (6% versus 1%) and for the insoluble portion to be more quickly converted to soluble with a faster reaction rate, as described in (Hamilton *et al* 2019, 2020, Rathod *et al* 2020).

The amount of Cl_2 produced from iron aerosols each timestep in a given grid box is a function of the incoming solar radiation at that time and place, divided by the solar radiation at Barbados from the observations of (Zhu *et al* 1997), multiplied by 11.4 photochemical cycles per hour, as measured by (Zhu *et al* 1997). While simple, this approach uses all available observations as much as possible and allows analysis to be extrapolated to other latitudes and seasons. Our approach gives a similar production of Cl_2 from mineral aerosols over the North Atlantic as (van Herpen *et al* 2023) which allowed the model to simulate measurements of CO isotopes (Mak 2003).

Third, we added the calculated molecular chlorine produced into the surface layer of the climate-chemistry version of CESM1-CAM4 (CAM4-chem). CAM4-chem includes a comprehensive representation of atmospheric chemistry including comprehensive halogen sources and chemistry (Li *et al* 2022). The simulations are run at a spatial resolution of 2.5° × 1.9° × 26 (longitude by latitude by vertical layers) using a prescribed SST and a standard land model. The boundary layer scheme is described in Hurrell *et al* (2013) and Park and Bretherton (2009). Additional chlorine sources are included in the model used in this study and are detailed in Li *et al* (2022). The model has an enhanced representations of natural short-lived halogens (Cl, Br, I) calculated online (Iglesias-Suarez *et al* 2020). Anthropogenic chlorine species and their processes are modeled based on (Keene William *et al* 1999, Hossaini *et al* 2016, Claxton *et al* 2020, Li *et al* 2022). The simulations are conducted within the CESM1 framework in a free running mode, using the prognostic weather and climate mode to capture atmospheric composition-climate feedbacks for 2020–2030, preceded by a 60 year spin-up (1960–2020). CH_4 is added by a transient emission inventory instead of lower boundary conditions, as described in Li *et al* (2022), to maintain free atmospheric chemical interactions of global methane. Li *et al* (2022) showed the global O_3 and tropospheric OH concentrations at the end of the spin-up period are in good agreement with observation and previous modeling studies. Molecular chlorine produced from iron is added as a surface emission with a diurnal cycle. We use other gas and aerosol emissions from 2020 to 2030 from the representative concentration pathway 8.5 (RCP8.5) as the main baseline scenario (henceforth designated as Base).

2.2. Scenario description

To understand the impact of additional molecular chlorine from iron aerosols in today's climate prior to any additional iron emissions (argued in (van Herpen *et al* 2023), and not included in current CESM models), we first simulate a baseline case using the present-day production of iron aerosols, as simulated in MIMI along with the parameterization of molecular chlorine production as discussed above. Present day iron emissions from maritime shipping are implemented in this default version of the model (Hamilton *et al* 2019, Rathod *et al* 2020). The resulting impact on methane gives similar results as (van Herpen *et al* 2023) (BASE case in table 1). From this base case, we introduce a series of scenarios to explore how interventions by adding additional iron aerosols impact atmospheric methane. In the first scenario, we assume additional iron emissions occur at a constant rate over all ocean surfaces (henceforth labeled as OC) (see table 1). We explore iron emissions in ship tracks (ST) in a second group of scenarios where we assume additional iron is emitted from maritime shipping activities. This would offer an efficient and readily available means of introducing additional iron into the atmosphere. We increase iron emissions in ship tracks, which are currently 2.2 Tg yr^{-1} in the base scenario by 100-, 500-, and 1,000 times henceforth labeled as ST100, ST500, and ST1000, respectively. Finally, in a group of box scenarios we restrict iron emissions to a regional box to better identify if there are particularly effective regions for emitting iron. In the box scenarios, we emit iron (kg m^{-2} s^{-1}) inside 10 × 10 model grid-boxes (1.25° × 0.9°) at one of three constant rates (henceforth labeled as low, mid, and high). The box emission regions are the North Pacific, North Atlantic, Southern Ocean, and equatorial Pacific (henceforth labeled as NP, NA, SO, and EP, respectively). We chose these regions in order to explore the importance of the efficiency of methane removal (discussed below), choosing some regions

Table 1. Scenario name designation, description and amount of iron added (Tg/yr).

Scenario group	Scenario name	Scenario description	Additional iron (Tg/yr)
	Base	Current-day iron emission	0
	OC	Iron over ocean surfaces	197
ST	ST100	100-times iron in ship tracks	18
	ST500	500-times iron in ship tracks	92
	ST1000	1000-times iron in ship tracks	185
Box	LowNP	Low iron emissions in the north Pacific	8
	MidNP	Medium iron emissions in the north Pacific	21
	HighNP	High iron emissions in the north Pacific	30
	LowNA	Low iron emissions in the north Atlantic	7
	MidNA	Medium iron emissions in the north Atlantic	16
	HighNA	High iron emissions in the north Atlantic	24
	LowSO	Low iron emissions in the Southern Ocean	5
	MidSO	Medium iron emissions in the Southern Ocean	14
	HighSO	High iron emissions in the Southern Ocean	20
	LowEP	Low iron emissions in the equatorial Pacific	7
	MidEP	Medium iron emissions in the equatorial Pacific	19
	HighEP	High iron emissions in the equatorial Pacific	28
Sensitivity	ST1000NoDiurnal	1000-times iron in ship tracks without diurnal cycle	185
	ST1000H1hr	HCl lifetime set to 1 h	185
	ST1000H12hr	HCl lifetime set to 12 h	185

that are more efficient (NP, NA, EP) and some that are less efficient (SO). We summarize all twenty simulated cases in table 1. In each case we assess both the iron aerosol production of Cl_2 and then the impact of the Cl_2 on the methane chemistry. For all these cases we assume that the additional iron emitted has the same solubility and atmospheric processing attributes as shipping iron, which starts much more soluble and is more easily solubilized than dust (Hamilton *et al* 2019). The chlorine production from the resulting photoactive iron is calculated as discussed above.

In order to show that our results are robust to our modeling assumptions, we performed three sensitivity tests of our approach with the ST1000 iron emission scheme. These scenarios are described in the supplementary information.

2.3. MAGICC description

In this paper we include only a 10 year simulation of the impact of iron additions on CH_4. However as this is not long enough to calculate the overall radiative effect, we extrapolate the 10 years of simulations to 2050 using the reduced-complexity Model for the Assessment of Greenhouse Gas Induced Climate Change version 6 (MAGICC6) (Meinshausen *et al* 2011a, 2011b) to simulate the change in radiative effects and surface temperature relative to 1850–1900 resulting from the different scenarios. In particular, we extrapolated the global percentage change of O_3 and CH_4 burden compared to the base scenario as given in the CAM4-chem simulations. MAGICC6 comprises four boxes representing land and ocean in both the northern and southern hemispheres. We drive MAGICC6 with RCP8.5 initial concentrations for most species and timeseries (2020–2050) but use the extrapolated ratios to change the surface CH_4 and O_3. To account for the iron RF, as calculated in MIMI, we use the percentage radiative change of iron (between the different scenarios and the Base scenario) and increase the black carbon (BC) aerosols in MAGICC6 to match the RF from added iron aerosols. Finally, we simulate the change in surface temperature and RF until 2050 across all scenarios. Our goal is to demonstrate the potential influence of these mitigation scenarios on surface temperature and RF, defining the change as the global surface temperature change relative to 1850 due to potential future iron emission additions. We use MAGICC because the lifetime of the aerosols is quite different than that of CH_4, and MAGICC allows us to calculate the impact of a long term addition of iron aerosols onto climate and extrapolate the CESM simulations from 10 years to the more climate relevant 30 years.

2.4. Methane removal efficiency calculation

To evaluate how effective the iron addition will be at removing methane, we introduce the concept of methane removal efficiency. We can define the efficiency either globally or locally. The global methane removal efficiency is given as:

$$Global\,Efficiency = \frac{\Delta\, total\, CH_4\, loss\, \left(Tg/_{yr}\right)}{\Delta\, iron\, flux\, \left(Tg/_{yr}\right)} \quad (1)$$

where the change in total CH_4 loss rate (Tg/yr) is the change in the global CH_4 loss rate over 10 years compared to the Base case, and the change in iron is the

total change in iron added from emissions in 10 years, or equivalently at steady state, the total amount of iron removed by deposition. Note that the change in methane burden from the base case includes changes from all chemical loss pathways due to iron addition (i.e. OH, Cl, and, photochemical reactions). The global efficiency gives an overall metric of the efficiency of the iron additions in destroying methane.

To identify where the iron additions would be most effective, we consider the efficiency calculated on a spatial basis. The spatial efficiency is calculated for each grid box as the change in column methane loss, divided by the change in iron flux in that grid box,

$$Spatial\,efficiency = \left.\frac{\Delta\, total\, CH_4\, loss\, \left(Tg/_{yr}\right)}{\Delta\, iron\, flux\, \left(Tg/_{yr}\right)}\right|_{\mathrm{lat,lon}} \quad (2)$$

Locally the iron flux could be calculated as the emission or the deposition of iron, and we explore the utility of using both metrics. While in the global simulation, at steady-state, the iron emissions and deposition are the same this is not true locally.

3. Results

3.1. Efficiency analysis

One immediate question that arises when considering iron addition is if there are some regions in which adding iron destroys more methane than other regions. We use constant emissions over the entire ocean (OC) scenario to calculate the spatial efficiency since the results are easier to interpret than other emission scenarios. The spatial efficiency reveals distinctly different spatial patterns when considered based on iron emission or deposition (figure 1(a) versus figure 1(c): equation (2). The efficiency based on emissions is solely determined by the methane loss since the emissions are constant (E2). This results in maximum (minimum) efficiency in regions of large methane losses (small methane losses). For example, the efficiency based on emissions (figure 1(a)) is comparatively high in the Pacific Inter Tropical Convergence Zone (ITCZ) where the EP box scenario is located (figure 1(a)), indicating large methane losses in this region. On the other hand, calculating the efficiency by dividing by the iron deposition rate instead (figure 1(d)) is dependent both on the methane loss and on the deposition rate. These results show that higher (lower) efficiency occurs in the regions with smaller (larger) deposition rates, or longer (shorter) iron lifetimes. In this case the high precipitation rates in the Pacific ITCZ (i.e. EP scenario) with its high rates of wet removal (figure 1(d)) result in a low efficiency. Since these two measures of efficiency give different results, we examine the methane removed by explicitly considering the different box scenarios, in the next section, where we show that using the deposition to define the efficiency locally better reflects the regional box results.

3.2. Variations in methane removal efficiency

Our analysis reveals significant regional variations in global methane removal efficiency (figure 2) depending on where the iron is emitted. The NP and NA scenarios have the most methane removed with additional iron emissions, indicating that specific regional dynamics, such as favorable locations for iron emissions and associated molecular chlorine production, can contribute the most to increased methane removal in these regions (figure 3). In contrast, the SO and EP scenarios have lower global methane removal (figure 2) with less chlorine produced per iron added (figure 3).

The removal efficiency is also impacted by the amount of iron added regionally. The nonlinear relationship between the addition of iron and methane is similar to that between chlorine and methane from other studies (Horowitz *et al* 2020, Li *et al* 2023) (figure 2). In all regions methane increases when additional iron emissions are low. The nonlinearity is caused by the additional produced Cl_2 reacting with both ozone and methane, where the reaction with ozone decreases the production of OH and thus increases CH_4, while the reaction with CH_4 decreases its concentration. When enough Cl2 has been produced, ozone becomes sufficiently decreased and no longer limits the reaction with methane, thereby effectively decreasing methane concentrations. Notably, even in the ST100 ship track scenario, where additional iron emissions are more than 16 times the current global combustion iron emissions, no visible decrease in methane burden was observed.

Also note, that at sufficient iron addition rates ($>$5–9 Tg $^{-1}$yr) the box scenarios all result in larger methane losses than the low ship-track (ST100) scenario, suggesting that focusing on one or two regions could be more efficient.

3.3. Regional efficiency variations

Next, we will discuss the reasons for the regional differences, focusing on the regional variations in chlorine production and its reactivity towards ozone and methane.

Chlorine production per emitted iron differs by over a factor of two between different regions (figure 3). Fundamentally the chlorine production depends on how photoactive the iron is, how long it lasts in the atmosphere, and the incoming solar radiation. The production ratio of Cl_2 to iron is 5:1 g Cl_2/g iron in the ship track scenario (figure 3). The scenario where iron is emitted constantly above the ocean (OC scenario—green circle in figure 3) gives

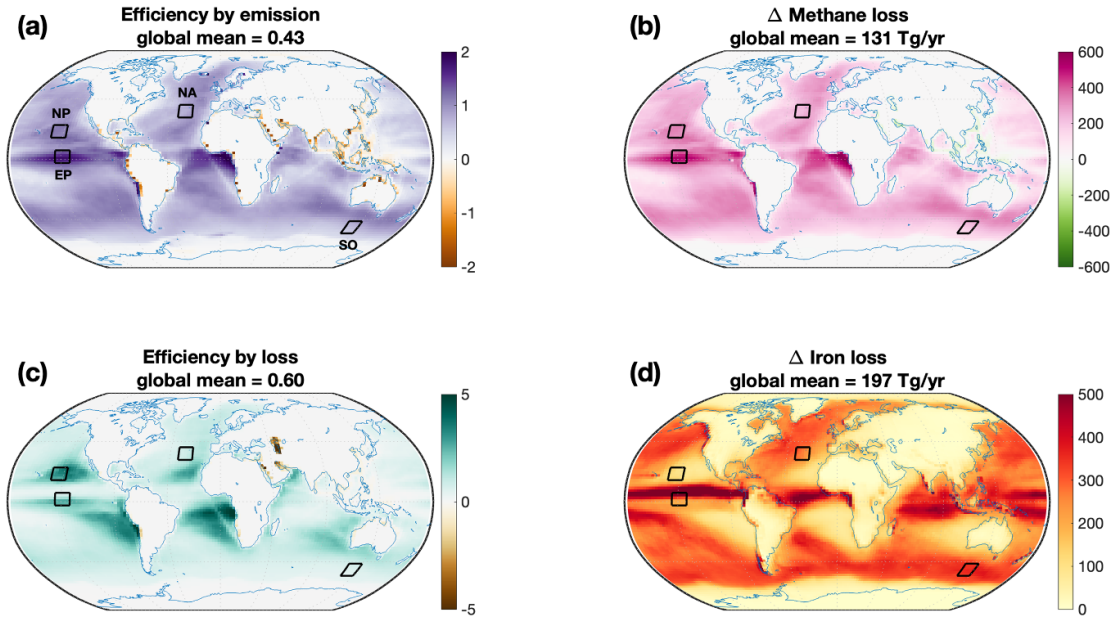

Figure 1. (a) Methane removal efficiency calculated by iron emission from the OC scenario following equation (2). (b) Change in total methane loss between OC scenario and Base scenario. (c) Methane removal efficiency calculated by iron loss from the OC scenario following equation (2). (d) Change in iron loss between OC scenario and Base scenario. The black boxes show the box scenarios NP, NA, SO, and EP, described in table 1, and labeled in figure (a). Figures S3, S4, and S10 show the absolute methane loss, methane burden, and iron loss (deposition) for all the scenarios.

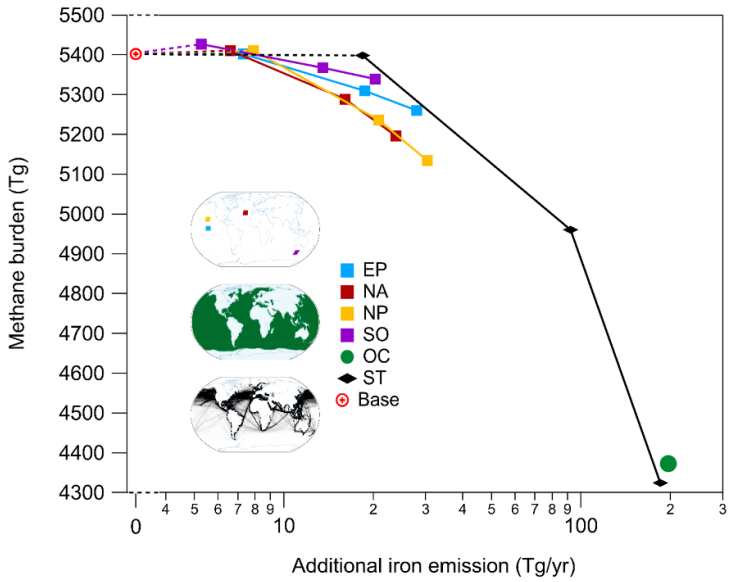

Figure 2. The relationship between the global methane burden after 10 years of intervention (Tg on vertical axis) and the additional iron emission (Tg/yr) for all the scenarios compared to Base scenario. The scenarios are the three ST scenarios (black diamond), the OC scenario (green circle), and the colored squares which represent different regions (shown in the insert maps): EP (cyan), NA (maroon), NP (yellow), SO (purple). The zero point is inserted to the plot on a linear scale and the dashed lines are to emphasize the initial increase in methane burden.

similar results as the ST scenario (black diamonds in figure 3). However, emissions in the more efficient regions, such as the boxes in the North Atlantic (NA) and North Pacific (NP), results in a high Cl_2 production ratio that increases to 7:1 g Cl_2/g iron (figure 3). These efficient scenarios (boxes NA and NP) are then best predicted by those regions where the local efficiency is defined in terms of the iron loss rate (figure 1(c)). This again suggests the regions with small iron deposition loss are most efficient at removing methane, resulting in a longer iron lifetime and a greater production of Cl_2 from the iron. The fact that we do not see a strong dependence of Cl_2 production on incoming solar radiation between the NA and NP scenarios is likely because of the similar latitudes chosen.

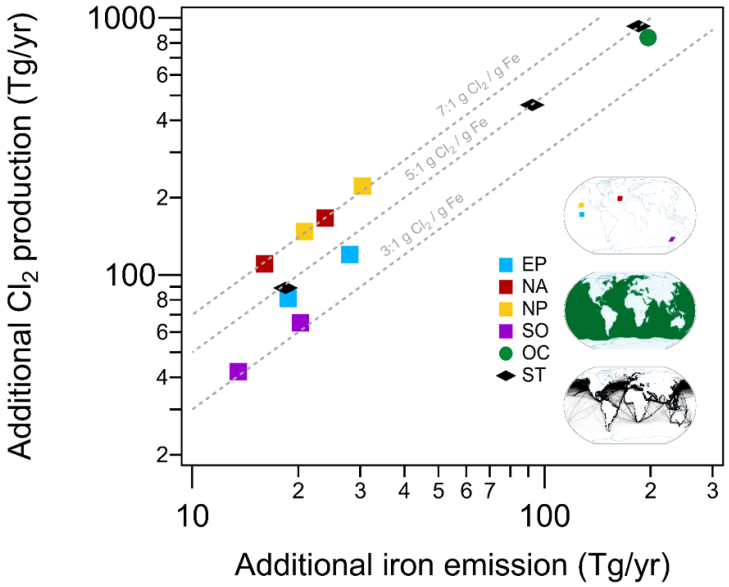

Figure 3. The relationship between additional Cl_2 production (vertical axis) and the additional iron emission (horizontal) for all the scenarios compared to Base scenario except for the scenarios with the nonlinear response, i.e. the low box scenarios (table 1). Dotted lines represent slopes deduced from the different cases, where the upper lines (7:1 gCl2/gFe) come from the more efficient NP and NA regions, while the lowest dotted lines (3:1 gCl2/gFe) come from the less efficient SO region. The same scenarios and color scale are used as in figure 2. Figures S5 and S11 show the Cl_2 produced and iron emission for all the scenarios.

The Cl_2 is assumed to be produced from a globally constant fraction of the soluble iron (as described in the methods) multiplied by the amount of insolation at a given location. Consequently, even globally constant rates of oceanic iron emissions (in the OC scenario), will not result in constant Cl_2 emissions (as was assumed in (Li *et al* 2023)), since the iron is removed at unequal rates, there are differences in soluble iron composition, and there are differences in insolation (figure 1(d)).

The efficiency of methane removal from iron addition between different regions is also impacted by the extent to which chlorine reacts with methane or with ozone as demonstrated previously in (Li *et al* 2023). Therefore, the global emission scenarios (OC and ST) are less efficient at removing methane per added iron, consistent with the fact that global ozone should be removed before the chlorine effectively reacts with methane.

$$Cl + CH_4 \xrightarrow{O_2} CH_3O_2 + HCl \quad (R1)$$

$$Cl + O_3 \rightarrow ClO + O_2 \quad (R2)$$

We define the chlorine reactivity sensitivity (CRS) as the rate chlorine reacts with ozone divided by the rate at which it reacts with methane:

$$Chlorine\,Reactivity\,Sensitivity = \frac{k_{Cl+O_3} * [O_3]}{k_{Cl+CH_4} * [CH_4]} \quad (3)$$

Chlorine reactivity towards ozone is higher where the ozone concentrations are higher (figure S6), i.e. in the northern hemisphere (figure 4(a)). The global averaged CRS shifts from $Cl + O_3$ dominated in the Base scenario (figure 4(a)) to a regime where the reaction of chlorine with ozone and methane are comparable in the ST1000 (figure 4(c)), HighNP (figure 4(d)), and HighNA (figure S7) scenarios. In the cases where iron is added locally in a box the CRS shifts towards a regime where $Cl + CH_4$ are highly favored locally (figure S7). However, as shown above the reactivity towards methane is not the prime determinant in the location of the most efficient regions, which is dominated by iron lifetime.

3.4. Future RF and surface temperature change

Here we consider the net impact of adding iron aerosols to the climate, using the output from the CESM models as well as the MAGICC model. When comparing the different scenarios to the Base scenario, the ozone RF decreases in all cases (figure 5), similar to what was seen in (Li *et al* 2022). In some cases, the methane burden and thus its RF also decreases (in the scenarios with higher iron emissions), while in other cases the methane burden and RF increases (figure 2). On the other hand, the presence of additional iron in the atmosphere, particularly in the form of iron oxides, has a warming effect on climate, although the strength of this warming is uncertain (Zhang *et al* 2015, Matsui *et al* 2018, Li *et al* 2021) (figure 5(b)). Notice that depending on where and how much iron is added there is a difference in the effects of iron aerosols on direct radiative effect (DRE) (figure 5(c)). For example, the difference between NP and EP in the iron direct effect is a result of the overall albedo change produced by the aerosols, which is very

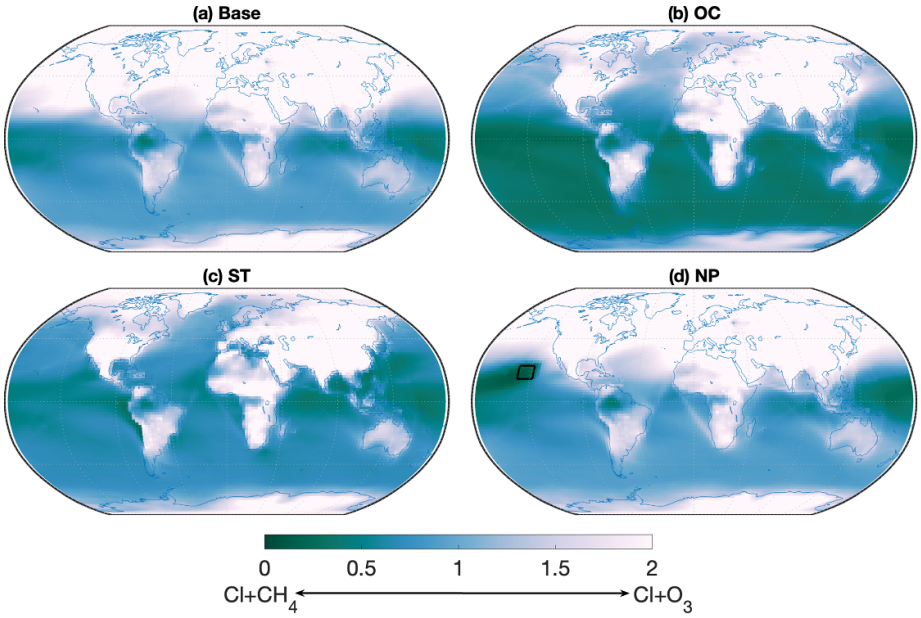

Figure 4. Chlorine reactivity towards ozone over reactivity towards methane (E3) in the troposphere for: (a) Base scenario, (b) OC scenario, (c) ST1000 scenario, and (d) HighNP scenario. Green colors indicate more Cl reactivity towards methane, and white colors indicate more Cl reactivity towards ozone. The black box represents the emission box in the NP scenario. Figure S7 shows the chlorine reactivity towards ozone over reactivity towards methane in the troposphere for all the scenarios.

sensitive to the background albedo (including cloud distribution and land surface).

The addition of iron decreases the overall RF in the NP scenario the most due to comparatively large decreases in the RF due to O_3 and CH_4 removal and comparatively small increases in the direct effect from the iron additions. However, adding iron does not always result in a net cooling because of increased iron aerosol solar absorption (figure 5). In all EP scenarios (i.e. low, mid, and high), the increase in DRE attributable to iron is higher than the decrease in RF due to the combined effects of ozone and methane (figure 5(b)). Adding iron in the HighEP scenarios increases the RF the most of all the scenarios examined compared to the base case due to the warming from the iron aerosols (figure 5(b)). In all low scenarios there is an increase in the methane-related RF but this is often compensated for by the decrease in the ozone RF.

Overall, in most scenarios, the increase in RF directly attributable to iron partially or wholly masks the beneficial reduction resulting from ozone and methane loss (figure 5(b)). In all cases, the resulting changes in surface temperatures by 2050 are very small across all scenarios (figure S8). Even in the highest scenarios analyzed, ST1000 and OC, in which almost 200 Tg of iron are added, the surface temperature reduction is, at most, approximately a tenth of a degree (figure S8). The uncertainties in MAGICC for surface temperature in the 2050 are large and increase in 2100 (Beusch *et al* 2022). The projected temperature uncertainties are as high as a degree, therefore, the highest modeled value of 0.12 °C decrease in the ST1000 scenario is not a significant change.

Although well studied, there is a very large uncertainty in ACIs for anthropogenic aerosols, as can also be seen in the latest IPCC report where the uncertainty in the effect of ACI is as large as the effect itself (Kikstra *et al* 2022). In this study we focus on the unique response to adding iron aerosols. Quantifying the effect of ACI on the global radiation budget carries a significantly larger uncertainty compared to the DRE of methane, ozone or iron aerosols, although the magnitude of ACI effect may well swamp the impact of adding iron specifically (figure S9). Thus, we do not include the impact of ACI of the additional anthropogenic aerosols into our MAGIC simulations, although this should be explored in the future. Additionally, absorbing aerosols like iron aerosols might also result in cloud burn-off (Fan *et al* 2016), but this effect is not included in our simulation.

3.5. Scenario overview

The CH_4 removed per Cl_2 produced maximizes at approximately 0.12 (Tg/Tg) with large iron additions in most of the scenarios examined (table 2). However, the maximum amount of CH_4 removed per iron added is very sensitive to the particular scenario, with the most efficient scenarios the boxes in the North Pacific and North Atlantic regions. This is due to iron losses as discussed in the regional efficiency variations section. These are also the most efficient scenarios for the Cl_2 produced per iron added and for the net climate effect of iron additions. However, despite

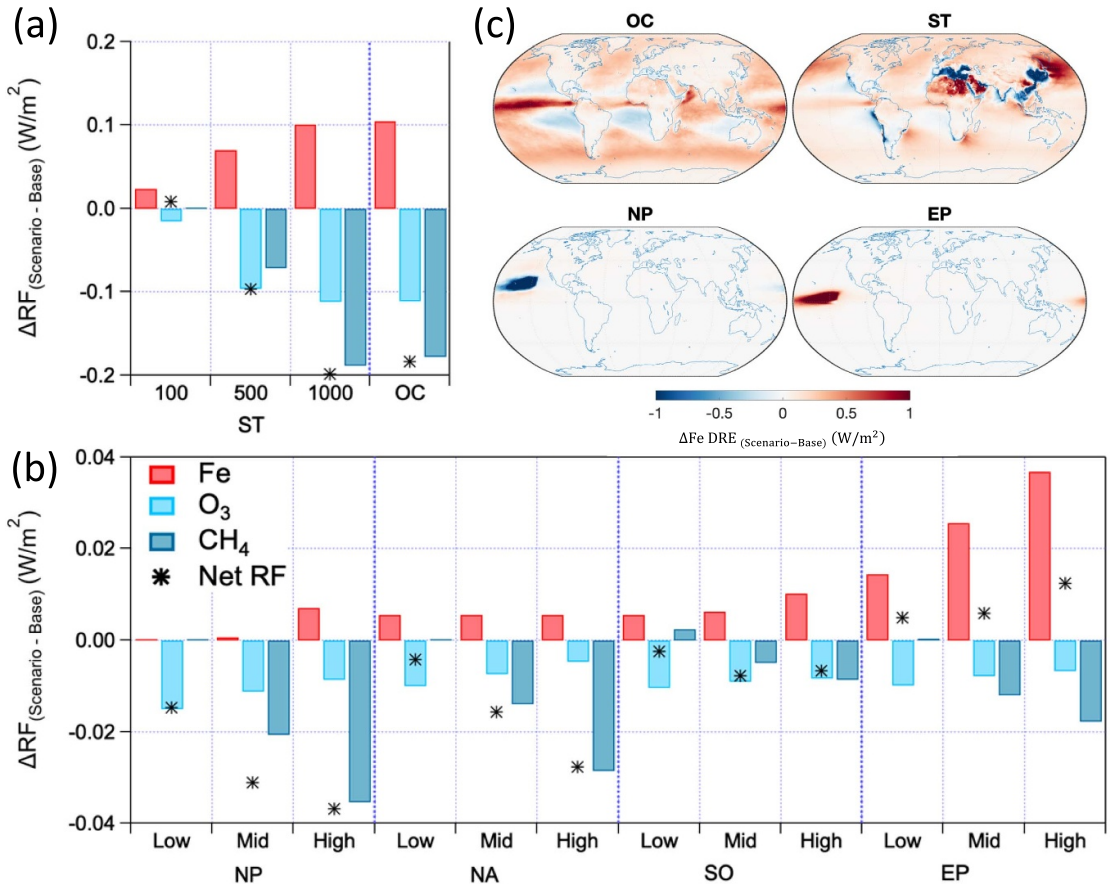

Figure 5. (a), and (b) change in DRE compared to the base scenario using MAGICC in the year 2050 for iron (red), ozone (light blue), methane (dark blue), and the net radiative change (asterisk). (c) Change in spatial iron DRE compared to the base scenario using CESM in the highest additions of the shown scenarios. Note the difference in *y*-axis scale.

Table 2. Result summary showing the methane removed over iron added (equation (1)), global and annual mean iron addition, change in net RF over iron emission, Cl_2 production over iron emission, methane removed over Cl_2 added.

Scenario name	$\frac{CH_4\ removed^a}{Total\ iron\ added^a}\left(\frac{Tg}{Tg}\right)$	*Iron added* $\left(\frac{Tg}{yr}\right)$	$\frac{Change\ in\ net\ RF}{Iron\ added}\left(\frac{mW/m^2}{Tg/yr}\right)$	$\frac{Cl_2\ produced}{Iron\ added}\left(\frac{Tg/yr}{Tg/yr}\right)$	$\frac{(CH_4\ removed)}{(Total\ Cl_2\ produced^a)}\left(\frac{Tg}{Tg}\right)$
OC	0.5	197	−0.9	4.3	0.12
ST100	0.0	18	0.5	4.8	0.00
ST500	0.5	92	−1.0	5.0	0.10
ST1000	0.6	185	−1.1	5.0	0.12
lowNP	−0.1	8	−1.9	1.3	−0.09
midNP	0.8	21	−1.5	7.1	0.11
highNP	0.9	30	−1.2	7.3	0.12
lowNA	−0.1	7	−0.6	4.4	−0.03
midNA	0.7	16	−1.0	6.9	0.10
highNA	0.9	24	−1.2	7.0	0.12
lowSO	−0.5	5	−0.5	1.8	−0.27
midSO	0.3	14	−0.6	3.1	0.08
highSO	0.3	20	−0.3	3.2	0.10
lowEP	0.0	7	0.7	2.7	0.00
midEP	0.5	19	0.3	4.3	0.11
highEP	0.5	28	0.4	4.3	0.12

[a] Methane removed refers to the methane removed after 10 years, total iron added and total Cl_2 produced refers to the total amount added/produced in 10 years.

somewhat lower efficiencies in CH_4 removed per added iron the ST1000 scenario is almost as effective in the net climate effect of iron additions. However, despite their efficiency, the net change in RF (table S2) and surface temperature by 2050 remain relatively low (figure S8).

4. Summary and conclusions

In this paper we focus on the challenge of mitigating atmospheric methane to combat climate change by investigating enhanced oxidation of methane interventions by artificially adding iron aerosols to the marine boundary layer. This intervention has the potential to decrease methane levels through enhanced molecular chlorine production. However, the potential trade-offs associated with such intervention are large (figure 5, table 2) as the added iron aerosol also increases the direct effect. We utilized a set of well-characterized CESM models to assess the efficacy and climate implications of such an approach. Spatial analyses revealed that adding iron aerosols in some regions such as the boxes in the North Atlantic and North Pacific are more likely to remove methane the most effectively while adding iron aerosols to a box in the Southern Ocean and Equatorial Pacific are likely to have very low methane removal efficiencies. Note that the regional boxes may not be representative of the full ocean basins, as the iron loss shown in figure 1(d).

We show that the reactivity of chlorine towards methane and ozone influences the efficiency of methane removal in different regions, but the lifetime of the iron in the atmosphere is the most important control on efficiency. Although iron emissions contribute to decreasing methane and ozone concentrations, the overall impact on RF and surface temperatures by 2050 remains relatively modest (a reduction of 0.12 °C in the highest ship track scenario) across all scenarios, even though up to 200 Tg yr^{-1} of iron aerosols are added (60 times current combustion iron emissions). Part of this modest result is because the added iron aerosols absorb solar radiation, thus partially offsetting the benefits of removing methane and ozone.

Further research is needed on many topics (see supplement for a discussion of main uncertainties), especially the sensitivity of our result to the photoactive portion of iron that is added. The impact of the iron deposition on ocean fertilization is briefly discussed in the SI but is also an important outcome of such iron-based strategy. The stratospheric chlorine injection due to the different scenarios will also affect the stratospheric ozone and the ozone hole. This will be better quantified with a fully aerosol-gas coupled model. In addition, there is likely to be a strong dependence of the efficiency on the details of the location and timing of the iron addition which needs more exploration. Overall, a better understanding of the positive and negative implications of adding iron aerosols and the resulting chlorine gas is vital to advance our understanding of effective iron-based strategies to mitigate atmospheric methane.

Our findings indicate that while there may be some localized enhancements in methane reduction due to very large iron additions (>60 Tg yr^{-1} of iron aerosols or at least 10–17 times global current combustion iron emission depending on the emission scenario), the scalability, global effectiveness, and environmental impacts of this method as a methane mitigation strategy remain uncertain.

Data availability statement

The data that support the findings of this study are openly available at the following URL/DOI: 10.17632/v6mmbm75wd.1 (Meidan 2023).

Acknowledgments

D M, N M M, and P H would like to acknowledge the support of Silverlining and Spark Climate Solutions. M S J and M v H would like to acknowledge support from Silverlining and Spark Climate Solutions. This material is based upon work supported by National Center for Atmospheric Research (NCAR), which is a major facility sponsored by NSF under the Cooperative Agreement 1852977. Computing resources, support, and data storage were provided by the Climate Simulation Laboratory at NCAR's Computational and Information Systems Laboratory (CISL), sponsored by the NSF. We thank the helpful suggestions from Spark Climate Solutions.

Conflict of interest

The University of Copenhagen (UCPH) has filed a patent application related to atmospheric iron chlorides on behalf of its inventors (M v H, M S J). All other authors declare they have no competing interests.

ORCID iDs

Matthew S Johnson https://orcid.org/0000-0002-3645-3955
Douglas S Hamilton https://orcid.org/0000-0002-8171-5723

References

Beusch L, Nicholls Z, Gudmundsson L, Hauser M, Meinshausen M and Seneviratne S I 2022 From emission scenarios to spatially resolved projections with a chain of computationally efficient emulators: coupling of MAGICC (v7.5.1) and MESMER (v0.8.3) *Geosci. Model. Dev.* **15** 2085–103

Carslaw K S 2022 Aerosol in the climate system *Aerosols and Climate* ed K S Carslaw (Elsevier) ch 2, pp 9–52 (available at: www.sciencedirect.com/science/article/pii/B9780128197660000080)

Chen Y and Siefert R L 2003 Determination of various types of labile atmospheric iron over remote oceans *J. Geophys. Res. Atmos.* **108** 4774

Claxton T *et al* 2020 A synthesis inversion to constrain global emissions of two very short lived chlorocarbons: dichloromethane, and perchloroethylene *J. Geophys. Res. Atmos.* **125** e2019JD031818

Conway T M, Hamilton D S, Shelley R U, Aguilar-Islas A M, Landing W M, Mahowald N M and John S G 2019 Tracing and constraining anthropogenic aerosol iron fluxes to the North Atlantic Ocean using iron isotopes *Nat. Commun.* **10** 2628

Danabasoglu G *et al* 2020 The community earth system model version 2 (CESM2) *J. Adv. Model. Earth Syst.* **12** e2019MS001916

Dietrich Oeste F, De Richter R, Ming T and Caillol S 2017 Climate engineering by mimicking natural dust climate control: the iron salt aerosol method *Earth Syst. Dyn.* **8** 1–54

Eyring V, Bony S, Meehl G A, Senior C A, Stevens B, Stouffer R J and Taylor K E 2016 Overview of the coupled model intercomparison project phase 6 (CMIP6) experimental design and organization *Geosci. Model. Dev.* **9** 1937–58

Fan J, Wang Y, Rosenfeld D and Liu X 2016 Review of aerosol–cloud interactions: mechanisms, significance, and challenges *J. Atmos. Sci.* **73** 4221–52

Hamilton D S *et al* 2019 Improved methodologies for Earth system modelling of atmospheric soluble iron and observation comparisons using the mechanism of intermediate complexity for modelling iron (MIMI v1.0) *Geosci. Model Dev.* **12** 3835–62

Hamilton D S *et al* 2022 Earth, wind, fire, and pollution: aerosol nutrient sources and impacts on ocean biogeochemistry *Annu. Rev. Mar. Sci.* **14** 303–30

Hamilton D S *et al* 2023 An aerosol odyssey: navigating nutrient flux changes to marine ecosystems *Elem. Sci. Anth.* **11** 00037

Hamilton D S, Scanza R A, Rathod S D, Bond T C, Kok J F, Li L, Matsui H and Mahowald N M 2020 Recent (1980–2015) trends and variability in daily-to-interannual soluble iron deposition from dust, fire, and anthropogenic sources *Geophys. Res. Lett.* **47** e2020GL089688

Horowitz H M *et al* 2020 Effects of sea salt aerosol emissions for marine cloud brightening on atmospheric chemistry: implications for radiative forcing *Geophys. Res. Lett.* **47** e2019GL085838

Hossaini R, Chipperfield M P, Saiz-Lopez A, Fernandez R, Monks S, Feng W, Brauer P and von Glasow R 2016 A global model of tropospheric chlorine chemistry: organic versus inorganic sources and impact on methane oxidation *J. Geophys. Res. Atmos.* **121** 14,214–271,297

Hurrell J W *et al* 2013 The community earth system model: a framework for collaborative research *Bull. Am. Meteorol. Soc.* **94** 1339–60

Iglesias-Suarez F, Badia A, Fernandez R P, Cuevas C A, Kinnison D E, Tilmes S, Lamarque J-F, Long M C, Hossaini R and Saiz-Lopez A 2020 Natural halogens buffer tropospheric ozone in a changing climate *Nat. Clim. Change* **10** 147–54

Intergovernmental Panel on Climate Change (IPCC) 2023 *Climate Change 2021—the Physical Science Basis: Working Group I Contribution to the Sixth Assessment Report of the Intergovernmental Panel on Climate Change* (Cambridge University Press) (available at: www.cambridge.org/core/books/climate-change-2021-the-physical-science-basis/415F29233B8BD19FB55F65E3DC67272B)

IPCC Core writing team 2023 Summary for policymakers *Climate Change 2023: Synthesis Report*

IPCC 2021 Summary for Policymakers *Climate Change 2021: The Physical Science Basis. Contribution of Working Group I to the Sixth Assessment Report of the Intergovernmental Panel on Climate Change* ed V Masson-Delmotte *et al* (Cambridge University Press) pp 3–32

Ito A *et al* 2019 Pyrogenic iron: the missing link to high iron solubility in aerosols *Sci. Adv.* **5** eaau7671

Ito A and Miyakawa T 2023 Aerosol iron from metal production as a secondary source of bioaccessible iron *Environ. Sci. Technol.* **57** 4091–100

Ito A, Ye Y, Baldo C and Shi Z 2021 Ocean fertilization by pyrogenic aerosol iron *npj Clim. Atmos. Sci.* **4** 30

Jickells T D *et al* 2005 Global iron connections between desert dust, ocean biogeochemistry, and climate *Science* **308** 67–71

Keene William C *et al* 1999 Composite global emissions of reactive chlorine from anthropogenic and natural sources: reactive chlorine emissions inventory *J. Geophys. Res. Atmos.* **104** 8429–40

Kikstra J S *et al* 2022 The IPCC Sixth Assessment Report WGIII climate assessment of mitigation pathways: from emissions to global temperatures *Geosci. Model Dev.* **15** 9075–109

Li L *et al* 2021 Quantifying the range of the dust direct radiative effect due to source mineralogy uncertainty *Atmos. Chem. Phys.* **21** 3973–4005

Li Q *et al* 2023 Global environmental implications of atmospheric methane removal through chlorine-mediated chemistry-climate interactions *Nat. Commun.* **14** 4045

Li Q, Fernandez R P, Hossaini R, Iglesias-Suarez F, Cuevas C A, Apel E C, Kinnison D E, Lamarque J-F and Saiz-Lopez A 2022 Reactive halogens increase the global methane lifetime and radiative forcing in the 21st century *Nat. Commun.* **13** 2768

Lim S S, Vos T, Flaxman A D, Danaei G, Shibuya K, Adair-Rohani H and AlMazroa M 2012 A comparative risk assessment of burden of disease and injury attributable to 67 risk factors and risk factor clusters in 21 regions, 1990−2010: a systematic analysis for the global burden of disease study 2010 *Lancet* **380** 2224–60

Liu M, Matsui H, Hamilton D S, Lamb K D, Rathod S D, Schwarz J P and Mahowald N M 2022 The underappreciated role of anthropogenic sources in atmospheric soluble iron flux to the Southern Ocean *npj Clim. Atmos. Sci.* **5** 28

Liu X, Ma P L, Wang H, Tilmes S, Singh B, Easter R C, Ghan S J and Rasch P J 2016 Description and evaluation of a new four-mode version of the modal aerosol module (MAM4) within version 5.3 of the community atmosphere model *Geosci. Model. Dev.* **9** 505–22

Mahowald N M *et al* 2008 Atmospheric iron deposition: global distribution, variability, and human perturbations *Ann. Rev. Mar. Sci.* **1** 245–78

Mahowald N M, Hamilton D S, Mackey K R M, Moore J K, Baker A R, Scanza R and Zhang Y 2018 Aerosol trace metal deposition dissolution and impacts on marine microorganisms and biogeochemistry *Nat. Commun.* **81** 1–15

Mak J E 2003 The seasonally varying isotopic composition of the sources of carbon monoxide at Barbados, West Indies *J. Geophys. Res.* **108** 4635

Matsui H, Mahowald N M, Moteki N, Hamilton D S, Ohata S, Yoshida A, Koike M, Scanza R A and Flanner M G 2018 Anthropogenic combustion iron as a complex climate forcer *Nat. Commun.* **9** 1593

Meidan D 2023 Evaluating the potential of iron-based interventions in methane reduction and climate mitigation *Mendeley Data* **V1**

Meinshausen M, Raper S C B and Wigley T M L 2011a Emulating coupled atmosphere-ocean and carbon cycle models with a simpler model, MAGICC6—part 1: model description and calibration *Atmos. Chem. Phys.* **11** 1417–56

Meinshausen M, Wigley T M L and Raper S C B 2011b Emulating atmosphere-ocean and carbon cycle models with a simpler model, MAGICC6—part 2: applications *Atmos. Chem. Phys.* **11** 1457–71

Meyer-Oeste F-D 2010 Method for cooling the troposphere

Mikkelsen M K, Liisberg J B, van Herpen M M J W, Mikkelsen K V and Johnson M S 2024 Photocatalytic chloride-to-chlorine conversion by ionic iron in aqueous aerosols: a combined experimental, quantum chemical, and chemical equilibrium model study *Aerosol Res.* **2** 31–47

Mikkelsen M K, Liisberg J B, van Herpen M M J W, Mikkelsen K V and Johnson M S 2024 Photocatalytic chloride-to-chlorine conversion by ionic iron in aqueous aerosols: a combined experimental, quantum chemical, and chemical equilibrium model study *Aerosol. Res.* **2** 31–47

Moore C M M *et al* 2013 Processes and patterns of oceanic nutrient limitation *Nat. Geosci.* **6** 701–10

Moore K, Doney S C, Lindsay K, Mahowald N and Michaels Anthony F A F 2006 Nitrogen fixation amplifies the ocean biogeochemical response to decadal timescale variations in mineral dust deposition *Tellus* B **58** 560

Myriokefalitakis S *et al* 2018 Reviews and syntheses: the GESAMP atmospheric iron deposition model intercomparison study *Biogeosciences* **15** 6659–84

O'Grady C 2021 Methane removal seen as tool to slow warming; as nations look to cut emissions of the gas, some researchers want to pull it out of the air *Science* **374** 667–8

Park S and Bretherton C S 2009 The university of Washington shallow convection and moist turbulence schemes and their impact on climate simulations with the community atmosphere model *J. Clim.* **22** 3449–69

Rathod S D, Hamilton D S, Mahowald N M, Klimont Z, Corbett J J and Bond T C 2020 A mineralogy-based anthropogenic combustion-iron emission inventory *J. Geophys. Res. Atmos.* **125** e2019JD032114

Rienecker M M *et al* 2011 MERRA: NASA's modern-era retrospective analysis for research and applications *J. Clim.* **24** 3624–48

Saiz-Lopez A and von Glasow R 2012 Reactive halogen chemistry in the troposphere *Chem. Soc. Rev.* **41** 6448–72

Saunois M *et al* 2020 The global methane budget 2000–2017 *Earth Syst. Sci. Data* **12** 1561–623

Scanza R A, Hamilton D S, Perez Garcia-Pando C, Buck C, Baker A and Mahowald N M 2018 Atmospheric processing of iron in mineral and combustion aerosols: development of an intermediate-complexity mechanism suitable for earth system models *Atmos. Chem. Phys.* **18** 14175–96

Shi Z, Krom M D, Bonneville S, Baker A R, Jickells T D and Benning L G 2009 Formation of iron nanoparticles and increase in iron reactivity in mineral dust during simulated cloud processing *Environ. Sci. Technol.* **43** 6592–6

Staniaszek Z, Griffiths P T, Folberth G A, O'Connor F M, Abraham N L and Archibald A T 2022 The role of future anthropogenic methane emissions in air quality and climate *npj Clim. Atmos. Sci.* **5** 21

Sturtz T M, Jenkins P T and de Richter R 2022 Environmental impact modeling for a small-scale field test of methane removal by iron salt aerosols *Sustainability* **14** 14060

Tagliabue A, Bowie A R, Boyd P W, Buck K N, Johnson K S and Saito M A 2017 The integral role of iron in ocean biogeochemistry *Nature* **543** 51–59

Tilmes S *et al* 2016 Representation of the community earth system model (CESM1) CAM4-chem within the chemistry-climate model initiative (CCMI) *Geosci. Model. Dev.* **9** 1853–90

United Nations Environment Programme and Climate and Clean Air Coalition 2021 *GLOBAL METHANE ASSESSMENT Benefits and Costs of Mitigating METHANE Emissions* (United Nations Environment Programme)

van Herpen M M J W *et al* 2023 Photocatalytic chlorine atom production on mineral dust–sea spray aerosols over the North Atlantic *Proc. Natl Acad. Sci.* **120** e2303974120

Wang X *et al* 2019 The role of chlorine in global tropospheric chemistry *Atmos. Chem. Phys.* **19** 3981–4003

Wittmer J, Bleicher S and Zetzsch C 2015 Iron(III)-induced activation of chloride and bromide from modeled salt pans *J. Phys. Chem.* A **119** 4373–85

Wittmer J and Zetzsch C 2017 Photochemical activation of chlorine by iron-oxide aerosol *J. Atmos. Chem.* **74** 187–204

Zhang X L, Wu G J, Zhang C L, Xu T L and Zhou Q Q 2015 What is the real role of iron oxides in the optical properties of dust aerosols? *Atmos. Chem. Phys.* **15** 12159–77

Zhu X R, Prospero J M and Millero F J 1997 Diel variability of soluble Fe(II) and soluble total Fe in North African dust in the trade winds at Barbados *J. Geophys. Res. Atmos.* **102** 21297–305